

Broken-symmetry states and phase diagram of the lowest Landau level in bilayer graphene

E. V. Gorbar and V. P. Gusynin

Bogolyubov Institute for Theoretical Physics, 03680, Kiev, Ukraine

Junji Jia and V. A. Miransky

Department of Applied Mathematics, University of Western Ontario, London, Ontario N6A 5B7, Canada

(Dated: January 20, 2012)

Broken-symmetry quantum Hall (QH) states with filling factors $\nu = 0, \pm 1, \pm 2, \pm 3$ in the lowest Landau level in bilayer graphene are analyzed by solving the gap equation in the random phase approximation. It is shown that in the plane of electric and magnetic fields, the critical line, which separates the spin and layer polarized phases at $\nu = 0$, extends to the $\nu = \pm 1$ QH states. The amplitudes of the gaps in the $\nu = \pm 1, \pm 3$, and $\nu = \pm 2$ QH states are significantly smaller than the amplitude of the $\nu = 0$ gap, due to the separate filling of the $n = 0$ and $n = 1$ orbital Landau levels and the negative contribution of the Hartree term, respectively. It is shown that those values of the external electric field where the conductance is not quantized correspond to the minima of the gaps.

PACS numbers: 81.05.ue, 73.43.-f, 73.43.Cd

I. INTRODUCTION

Bilayer graphene is a new material with unique properties.¹⁻⁴ The possibility of inducing a tunable bandgap by top-bottom gates voltage makes it very promising for applications in various electronic devices.

Recent experiments in bilayer graphene⁵⁻¹⁰ revealed the generation of energy gaps in a magnetic field with complete lifting of the eightfold degeneracy in the zero energy (lowest) Landau level (LLL), which leads to new quantum Hall states with filling factors $\nu = 0, \pm 1, \pm 2, \pm 3$. While in Refs. 5,7,8,10 suspended bilayer graphene was used, bilayer graphene samples deposited on SiO₂/Si substrates were utilized in Refs. 6,9. Because suspended bilayer graphene is much cleaner than that on a substrate, the new quantum Hall states in the former start to develop at essentially smaller magnetic fields than in the latter. The theory of the quantum Hall (QH) effect in bilayer graphene has been studied in Refs. 11–20.

It was revealed in Ref. 5 that the energy gaps scale linearly with magnetic field B in bilayer graphene. It is unlike the case of monolayer graphene where a \sqrt{B} scaling for the gaps takes place.^{21,22} As was suggested in Refs. 15–17, a strong screening produced by the Coulomb interaction is responsible for this modification of the scaling in bilayer.²³ The physics underlying this effect is the following.^{16,17} Due to a nonrelativistic like dispersion relations for quasiparticles,¹ the polarization function in bilayer graphene in a magnetic field is strongly enhanced as compared to the case of monolayer graphene. In particular, it is proportional to the large mass of the quasiparticles $m \simeq 10^{-2}m_e$. Such a strong screening radically changes the form of the interaction and leads to the linear scaling.

Another interesting phenomenon in the $\nu = 0$ QH state in bilayer graphene is the phase transition between the spin polarized (ferromagnetic) phase and the layer polarized one in the BE_\perp -plane, where E_\perp is an electric field orthogonal to the bilayer planes. It was analyzed in theoretical studies in Refs. 16–19 and observed in experiments in Refs. 7,9,10.

The main conclusion of the analysis in Refs. 16,17 was that these two phases are separated by the critical line $\tilde{\Delta}_0 = \mu_B B + e^2 d/l^2$, where μ_B is the Bohr magneton, $l = \sqrt{\hbar c/eB}$ is the magnetic length, $\tilde{\Delta}_0 = eE_\perp d/2$ is the top-bottom gates voltage imbalance, and $d \simeq 0.35\text{nm}$ is the distance between the graphene layers. This critical line is qualitatively consistent with the experimental results in Refs. 7,9,10.

Only the $\nu = 0$ QH state was analyzed in Refs. 16–19. As to the QH states with $\nu = \pm 1, \pm 2, \pm 3$, the main experimental results obtained in Refs. 7,8 are the following: a) For $\nu = \pm 1$, there are two phases separated by approximately the same critical line as that in the $\nu = 0$ QH state. b) There is only one phase for $\nu = \pm 2$ and $\nu = \pm 3$ QH states. c) The $\nu = 0$ gap is approximately 30 – 40% larger than the $\nu = \pm 2$ one and significantly (by factor 10) exceeds the $\nu = \pm 1$ gap. d) For $\nu = 0$, $\nu = \pm 1$, $\nu = \pm 2$, and $\nu = \pm 3$, the conductance is quantized except at particular values of the electric field E_\perp .

In this paper we extend the analysis of Refs. 16,17 beyond the neutral point and describe the QH states with the filling factors $\nu = \pm 1, \pm 2, \pm 3$. As will be shown below, the results of the analysis reproduce correctly the main characteristics of the experimental data.

The paper is organized as follows. In Sec. II, the Hamiltonian of the model, its symmetries, and order parameters are described. In Sec. III, by using the Baym-Kadanoff formalism, the gap equation for the quasiparticle propagator

including the polarization function is derived. In Sec. IV, the properties of the solutions of the gap equation and the phase diagram of the LLL are described. In Sec. V, we compare our results with experiment. In Sec. VI, the main results of the paper are summarized. In Appendix we comment on the bare splitting of the Landau levels with orbital indices 0 and 1 induced by a bias electric field.

II. MODEL

We will utilize the same model for describing the low-energy electronic excitations as in Refs. 16,17. It can be derived from the more accurate four-band model, which takes into account the sombrero shape of the band structure for zero magnetic field.^{1,4,24} The free part of the effective low energy Hamiltonian of bilayer graphene is:¹

$$H_0 = -\frac{1}{2m} \int d^2x \Psi_{Vs}^\dagger(x) \begin{pmatrix} 0 & (\pi^\dagger)^2 \\ \pi^2 & 0 \end{pmatrix} \Psi_{Vs}(x), \quad (1)$$

where $\pi = \hat{p}_{x_1} + i\hat{p}_{x_2}$ and the canonical momentum $\hat{\mathbf{p}} = -i\hbar\nabla + e\mathbf{A}/c$ includes the vector potential \mathbf{A} corresponding to the external magnetic field \mathbf{B} . Without magnetic field, this Hamiltonian generates the spectrum $E = \pm \frac{p^2}{2m}$, where $m = \gamma_1/2v_F^2$ with the Fermi velocity $v_F \simeq c/300$ and $\gamma_1 \approx 0.34 - 0.40$ eV. The two component spinor field Ψ_{Vs} carries the valley ($V = K, K'$) and spin ($s = +, -$) indices. We will use the standard convention: $\Psi_{Ks}^T = (\psi_{A1}, \psi_{B2})_{Ks}$ whereas $\Psi_{K's}^T = (\psi_{B2}, \psi_{A1})_{K's}$. Here A_1 and B_2 correspond to those sublattices in the layers 1 (top) and 2 (bottom), respectively, which, according to Bernal ($A_2 - B_1$) stacking, are relevant for the low energy dynamics.

The Zeeman and Coulomb interactions plus a top-bottom gates voltage imbalance $\tilde{\Delta}_0$ in bilayer graphene are described as (henceforth we will omit indices V and s in the field Ψ_{Vs}):

$$\begin{aligned} H_{\text{int}} = & Z \int d^2x \Psi^\dagger(x) \sigma^3 \Psi(x) + \frac{1}{2} \int d^2x d^2x' \{ V(x-x') [\rho_1(x)\rho_1(x') + \rho_2(x)\rho_2(x')] + 2V_{12}(x-x')\rho_1(x)\rho_2(x') \} \\ & + \tilde{\Delta}_0 \int d^2x \Psi^\dagger(x) \xi \tau_3 \Psi(x) - \frac{\tilde{\Delta}_0}{m\gamma_1} \int d^2x \Psi^\dagger(x) \xi \begin{pmatrix} \pi^\dagger \pi & 0 \\ 0 & -\pi \pi^\dagger \end{pmatrix} \Psi(x), \end{aligned} \quad (2)$$

where σ^3 is a spin matrix, $Z \equiv \mu_B B = 0.67 B[\text{T}]\text{K}$ is the Zeeman energy, the Pauli matrix τ^3 in the voltage imbalance term acts on layer components, and $\xi = \pm 1$ for the valleys K and K' , respectively. The potential $V(x)$ describes the intralayer interactions and, therefore, coincides with the bare potential in monolayer graphene whose Fourier transform is given by $\tilde{V}(k) = 2\pi e^2/\kappa k$, where κ is the dielectric constant. The potential V_{12} describes the interlayer electron interactions. Its Fourier transform is $\tilde{V}_{12}(k) = (2\pi e^2/\kappa)(e^{-kd}/k)$. The two-dimensional charge densities $\rho_1(x)$ and $\rho_2(x)$ are:

$$\rho_1(x) = \Psi^\dagger(x) P_1 \Psi(x), \quad \rho_2(x) = \Psi^\dagger(x) P_2 \Psi(x), \quad (3)$$

where $P_1 = (1 + \xi\tau^3)/2$ and $P_2 = (1 - \xi\tau^3)/2$ are projectors on states in the layers 1 and 2, respectively. When the polarization effects are taken into account, the potentials $V(x)$ and $V_{12}(x)$ are replaced by effective interactions $V_{\text{eff}}(x)$ and $V_{12\text{eff}}(x)$. The last term in Eq.(2) leads to the splitting of the Landau levels with orbital indices $n = 0$ and $n = 1$.^{1,4,24} As is discussed in Appendix below, for the values of the magnetic field $B < 10\text{T}$, which are relevant for the experiment with suspended bilayer graphene^{7,8} and the present analysis, the contribution of this term is small. On the other hand, it could be relevant for stronger magnetic fields. Because of that, this term is omitted in the analysis of the gap equations in the main text, although we discuss some interesting features this term could lead to in the case of stronger magnetic fields in Secs. IV A - IV D and Appendix.

If both the Zeeman and $\tilde{\Delta}_0$ terms are ignored, the Hamiltonian $H = H_0 + H_{\text{int}}$, with H_0 and H_{int} in Eqs. (1) and (2), possesses the symmetry $G = U^{(K)}(2)_S \times U^{(K')}(2)_S \times Z_{2V}^{(+)} \times Z_{2V}^{(-)}$, where $U^{(V)}(2)_S$ defines the $U(2)$ spin transformations in a fixed valley $V = K, K'$, and $Z_{2V}^{(s)}$ describes the valley transformation $\xi \rightarrow -\xi$ for a fixed spin $s = \pm$.^{16,17} The Zeeman interaction lowers this symmetry down to $G_2 \equiv U^{(K)}(1)_+ \times U^{(K)}(1)_- \times U^{(K')}(1)_+ \times U^{(K')}(1)_- \times Z_{2V}^{(+)} \times Z_{2V}^{(-)}$, where $U^{(V)}(1)_s$ is the $U(1)$ transformation for fixed values of both valley and spin. Including the $\tilde{\Delta}_0$ term lowers the G_2 symmetry further down to the $\bar{G}_2 \equiv U^{(K)}(1)_+ \times U^{(K)}(1)_- \times U^{(K')}(1)_+ \times U^{(K')}(1)_-$.

The dynamics in the integer QH effect in bilayer graphene is intimately connected with dynamical breakdown of the G and G_2 symmetries. Two sets of the order parameters describing their breakdown were considered in Refs. 16,17. The first set consists of the quantum Hall ferromagnetism (QHF) order parameters:²⁵

$$\mu_s : \quad \langle \Psi_s^\dagger \Psi_s \rangle = \langle \psi_{KA_1s}^\dagger \psi_{KA_1s} + \psi_{K'A_1s}^\dagger \psi_{K'A_1s} + \psi_{KB_2s}^\dagger \psi_{KB_2s} + \psi_{K'B_2s}^\dagger \psi_{K'B_2s} \rangle, \quad (4)$$

$$\tilde{\mu}_s : \quad \langle \Psi_s^\dagger \xi \Psi_s \rangle = \langle \psi_{KA_1s}^\dagger \psi_{KA_1s} + \psi_{KB_2s}^\dagger \psi_{KB_2s} - \psi_{K'B_2s}^\dagger \psi_{K'B_2s} - \psi_{K'A_1s}^\dagger \psi_{K'A_1s} \rangle. \quad (5)$$

The order parameter (4) is the charge density for a fixed spin whereas the order parameter (5) determines the charge-density imbalance between the two valleys. The corresponding chemical potentials are μ_s and $\tilde{\mu}_s$, respectively.

The second set consists of the magnetic catalysis (MC) order parameters,²⁶ i.e., the Dirac $\tilde{\Delta}_s$ and Haldane Δ_s mass terms:

$$\Delta_s : \quad \langle \Psi_s^\dagger \tau_3 \Psi_s \rangle = \langle \psi_{KA_1s}^\dagger \psi_{KA_1s} - \psi_{KB_2s}^\dagger \psi_{KB_2s} + \psi_{K'B_2s}^\dagger \psi_{K'B_2s} - \psi_{K'A_1s}^\dagger \psi_{K'A_1s} \rangle, \quad (6)$$

$$\tilde{\Delta}_s : \quad \langle \Psi_s^\dagger \xi \tau_3 \Psi_s \rangle = \langle \psi_{KA_1s}^\dagger \psi_{KA_1s} + \psi_{K'A_1s}^\dagger \psi_{K'A_1s} - \psi_{KB_2s}^\dagger \psi_{KB_2s} - \psi_{K'B_2s}^\dagger \psi_{K'B_2s} \rangle. \quad (7)$$

Clearly, the order parameter (6) describes a charge density wave in both the K and K' valleys. While this order parameter preserves the G_2 symmetry, it is odd under time reversal.²⁷ On the other hand, the order parameter (7), connected with the conventional Dirac mass $\tilde{\Delta}_s$, determines the charge-density imbalance between the two layers.¹ Like the QHF order parameter (5), this mass term completely breaks the $Z_{2V}^{(s)}$ symmetry and is even under time reversal. It is important that in both monolayer and bilayer graphene, these two sets of the order parameters necessarily coexist^{16,17,28} and are produced even at the weakest repulsive interactions between electrons (magnetic catalysis²⁹⁻³¹). The essence of this phenomenon is an effective reduction by two units of the spatial dimension in the electron-hole pairing in the LLL with energy $E = 0$.

Let us also emphasize that unlike a spontaneous breakdown of continuous symmetries, a spontaneous breakdown of the discrete valley symmetry $Z_{2V}^{(s)}$, with the order parameters $\langle \Psi_s^\dagger \xi \Psi_s \rangle$ and $\langle \Psi_s^\dagger \xi \tau_3 \Psi_s \rangle$, is not forbidden by the Mermin-Wagner theorem at finite temperatures in a planar system.³² Also, because the valley and layer indices are equivalent in the LLL,¹ these order parameters also describe a breakdown of the symmetry between the top and bottom layers.

Note that because of the Zeeman interaction, the $SU^{(V)}(2)_S$ is explicitly broken, leading to a spin gap. This gap could be dynamically strongly enhanced³³. In that case, a quasispontaneous breakdown of the $SU^{(V)}(2)_S$ takes place. The corresponding ferromagnetic phase is described by the chemical potential $\mu_3 = (\mu_+ - \mu_-)/2$, corresponding to the QHF order parameter $\langle \Psi^\dagger \sigma_3 \Psi \rangle$, and by the mass $\Delta_3 = (\Delta_+ - \Delta_-)/2$ corresponding to the MC order parameter $\langle \Psi^\dagger \tau_3 \sigma_3 \Psi \rangle$.

Recall also that in bilayer graphene, the LLL includes both the $n = 0$ and $n = 1$ LLs, if the Coulomb interaction is ignored.¹ Therefore, in the LLL approximation, there is an approximate orbital symmetry Z_{2L} connected with a $n = 0 \rightarrow n = 1$ transformation.

III. GAP EQUATION

The gap equation for the full propagator G in the LLL approximation in bilayer graphene was derived in Ref. 17. In the derivation, the Baym-Kadanoff (BK) formalism³⁴ was utilized. In this section, we describe the main features of the gap equation. Note that because a characteristic scale in the bilayer dynamics in a magnetic field is the cyclotron energy $\hbar\omega_c \simeq 2.19B[\text{T}]\text{meV}$, the applicability of the LLL approximation implies that the LLL energy gaps should be smaller than $\hbar\omega_c$. As we will see, this condition is fulfilled in bilayer graphene.

We will analyze the gap equation for the full quasiparticle propagator G with the order parameters introduced in Eqs. (4)-(7). The mean field approximation with the polarization function calculated in the random phase approximation (RPA) will be used. The corresponding two-loop BK effective action is a functional of the full quasiparticle propagator G and it has the form:¹⁷

$$\Gamma(G) = \Gamma_0(G) + \Gamma_2(G), \quad \Gamma_0(G) = -i \text{Tr} [\text{Ln} G^{-1} + S^{-1}G - 1], \quad (8)$$

where S is the free Green's function, Γ_0 is the free part, and Γ_2 takes into account the interaction effects in the first order of perturbation theory,

$$\begin{aligned} \Gamma_2(G) = & - \int d^3u d^3u' \left\{ \frac{1}{2} \text{tr} [G(u, u') G(u', u)] V_{\text{eff}}(u - u') + \text{tr} [P_1 G(u, u') P_2 G(u', u)] V_{\text{IL}}(u - u') \right. \\ & \left. - \frac{1}{2} \text{tr} [G(u, u)] \text{tr} [G(u', u')] V_{\text{eff}}(u - u') - \text{tr} [P_1 G(u, u)] \text{tr} [P_2 G(u', u')] V_{\text{IL}}(u - u') \right\}. \end{aligned} \quad (9)$$

Here $u \equiv (t, \mathbf{r})$, t is the time coordinate, $\mathbf{r} = (x, y)$, and $V_{\text{IL}}(u) = V_{12\text{eff}}(u) - V_{\text{eff}}(u)$ is a combination of the interlayer and intralayer interactions (recall that the polarization contributions are included in the potentials $V_{\text{eff}}(u)$ and $V_{12\text{eff}}(u)$). Note that while here the trace Tr , the logarithm, and the product $S^{-1}G$ are taken in the functional sense, the trace tr runs over layer, valley and spin indices. The stationary condition $\delta\Gamma/\delta G = 0$ leads to the gap equation for the quasiparticle propagator G in mean field approximation.

We will use the Landau gauge for a two dimensional vector potential, $\mathbf{A} = (0, Bx)$, where B is the component of the magnetic field \mathbf{B} orthogonal to the xy plane of graphene. Then, the free Green's function $S(u_1, u_2)$ can be written as a product of a translation invariant part $\tilde{S}(u_1 - u_2)$ times the Schwinger phase factor²⁹

$$S(u_1, u_2) = \exp\left(-i\frac{(x_1 + x_2)(y_1 - y_2)}{2l^2}\right) \tilde{S}(u_1 - u_2). \quad (10)$$

Similarly, we can separate the Schwinger phase factor from the translation invariant part in the full propagator

$$G(u_1, u_2) = \exp\left(-i\frac{(x_1 + x_2)(y_1 - y_2)}{2l^2}\right) \tilde{G}(u_1 - u_2). \quad (11)$$

For the LLL with the orbital numbers $n = 0, 1$, the translation invariant part of the time Fourier transform of the free propagator takes a simple form:

$$\tilde{S}_{\xi s}(\mathbf{r}; \omega) = \frac{1}{2\pi l^2} \exp\left(-\frac{\mathbf{r}^2}{4l^2}\right) \left[L_0\left(\frac{\mathbf{r}^2}{2l^2}\right) + L_1\left(\frac{\mathbf{r}^2}{2l^2}\right) \right] S_{\xi s}(\omega) P_- \quad (12)$$

with

$$S_{\xi s}(\omega) = \frac{1}{\omega + \mu_0 - sZ + \xi\tilde{\Delta}_0 + i\delta\text{sgn}\omega}, \quad (13)$$

where μ_0 is the electron chemical potential, Z is the Zeeman energy, and the projector $P_- = (1 - \tau_3)/2$.

Motivated by expression (12) for $\tilde{S}_{\xi s}(\mathbf{r}; \omega)$, we will use the following ansatz for the full propagator with the parameters $\mu_s(n)$, $\tilde{\mu}_s(n)$, $\Delta_s(n)$, and $\tilde{\Delta}_s(n)$ related to the order parameters in Eqs. (4) – (7):

$$\tilde{G}_{\xi s}(\mathbf{r}; \omega) = \frac{1}{2\pi l^2} \exp\left(-\frac{\mathbf{r}^2}{4l^2}\right) \left[G_{\xi 0s}(\omega) L_0\left(\frac{\mathbf{r}^2}{2l^2}\right) + G_{\xi 1s}(\omega) L_1\left(\frac{\mathbf{r}^2}{2l^2}\right) \right] P_-, \quad (14)$$

where

$$G_{\xi ns}(\omega) = \frac{1}{\omega - E_{\xi ns} + i\delta\text{sgn}\omega} \quad (15)$$

and

$$E_{\xi ns} = -(\mu_s(n) + \Delta_s(n)) + \xi(\tilde{\mu}_s(n) - \tilde{\Delta}_s(n)), \quad n = 0, 1, \quad (16)$$

are the energies of the LLL states depending on the parameters $\mu_s(n)$, $\tilde{\mu}_s(n)$, $\Delta_s(n)$, and $\tilde{\Delta}_s(n)$. Note that because for the LLL states only the component ψ_{B_2s} (ψ_{A_1s}) of the wave function at the K (K') valley is nonzero, their energies depend only on the eight independent combinations of the QHF and MC parameters shown in Eq. (16).³⁵ Our goal is to find the energies $E_{\xi ns}$ from the gap equation.

It is convenient to solve the gap equation in momentum space. Then, the Fourier transform $\tilde{V}_{\text{eff}}(\omega, k)$ of $V_{\text{eff}}(u)$ is:¹⁷

$$\tilde{V}_{\text{eff}}(\omega, k) = \frac{2\pi e^2}{\kappa} \frac{1}{k + \frac{4\pi e^2}{\kappa} \Pi(\omega, \mathbf{k}^2)} \quad (17)$$

with $\Pi(\omega, k^2) \equiv \Pi_{11}(\omega, \mathbf{k}) + \Pi_{12}(\omega, \mathbf{k})$, where the polarization function Π_{ij} describes electron densities correlations on the layers i and j in a magnetic field. For the polarization function $\Pi(\omega, k^2)$ we use the expression in the RPA approximation modified by the presence of a quasiparticle bare gap $\tilde{\Delta}_0$ term (see Eq.(A24) in Ref. 17). As to the potential $V_{\text{IL}}(u)$, the gap equation contains its Fourier transform only at zero frequency and momentum:¹⁷

$$\tilde{V}_{\text{IL}}(\omega = 0, k = 0) = -\frac{2\pi e^2 d}{\kappa}. \quad (18)$$

The inclusion of the polarization effects is crucial for ensuring the linear scaling in bilayer graphene. We utilize the frequency independent order parameters $\mu, \tilde{\mu}, \Delta, \tilde{\Delta}$ and the static approximation for the polarization function will be used, $\Pi(\omega, \mathbf{k}^2) \rightarrow \Pi(0, \mathbf{k}^2)$.³⁶ The explicit expression for the polarization function calculated in the RPA approximation can be found in Ref. 17.

Using the ansatz (14), one finds that the gap equation $\delta\Gamma/\delta G = 0$ leads to the following system of equations for the energies $E_{\xi sn}$ (for details, see Ref. [17]):

$$\begin{aligned} -E_{\xi 0s} &= \mu_0 - sZ + \xi\tilde{\Delta}_0 - \frac{\hbar^2}{2ml^2} [\text{sgn}(E_{\xi 0s}) I_1(x) + \text{sgn}(E_{\xi 1s}) I_2(x)] \\ &+ \frac{1}{4\pi l^2} \left[(A_1 + A_2) \tilde{V}_{\text{eff}}(0) + \left(\frac{1-\xi}{2} A_2 + \frac{1+\xi}{2} A_1 \right) \tilde{V}_{\text{IL}}(0) \right], \end{aligned} \quad (19)$$

$$\begin{aligned} -E_{\xi 1s} &= \mu_0 - sZ + \xi\tilde{\Delta}_0 - \frac{\hbar^2}{2ml^2} [\text{sgn}(E_{\xi 0s}) I_2(x) + \text{sgn}(E_{\xi 1s}) I_3(x)] \\ &+ \frac{1}{4\pi l^2} \left[(A_1 + A_2) \tilde{V}_{\text{eff}}(0) + \left(\frac{1-\xi}{2} A_2 + \frac{1+\xi}{2} A_1 \right) \tilde{V}_{\text{IL}}(0) \right], \end{aligned} \quad (20)$$

where the integrals $I_i(x)$ are

$$I_i(x) = \int_0^\infty \frac{dy f_i(y) e^{-y}}{\kappa\sqrt{xy} + 4\pi\tilde{\Pi}(y)} \quad (21)$$

with $f_i(y) = (1, y, (1-y)^2)$ for $i = 1, 2, 3$, respectively. Here the dimensionless variable $x = 2\hbar^4/e^4 m^2 l^2 = (4\hbar\omega_c/\alpha^2\gamma_1)(v_F/c)^2 \simeq 0.003B[\text{T}]$, where $\alpha = 1/137$ is the fine-structure constant and we used the values $\gamma_1 = 0.39\text{eV}$, $\hbar\omega_c = \hbar^2/ml^2 = 2.19B[\text{T}]\text{meV}$, $v_F = 8.0 \times 10^5 \text{m/s}$ (see Ref. 1). The quantities A_1 and A_2 are $A_1 = \sum_{n,s} \text{sgn}(E_{-1ns})$, $A_2 = \sum_{n,s} \text{sgn}(E_{1ns})$.

The terms in the first and second square brackets on the right hand side of Eqs. (19) and (20) describe the exchange and Hartree contributions, respectively. In the latter, the terms with the factor $(A_1 + A_2)/4\pi l^2$ are proportional to $\text{tr}[G(0)]$,¹⁷ i.e., the density of charge carriers. There are other Hartree contributions, such as those taking into account the background charge of ions in graphene, the charge in the substrate, etc., which are not included in the equations. Due to the overall neutrality of the system, all these contributions should exactly cancel. As a result, only the Hartree terms with the factor $(A_1 - A_2)/4\pi l^2$ survive. They describe the capacitor like interactions in bilayer graphene. Thus, the final equations, taking into account the neutrality condition, are:

$$E_{\xi 0s} = -\mu_0 + sZ - \xi\tilde{\Delta}_0 + \frac{\hbar^2}{2ml^2} [\text{sgn}(E_{\xi 0s}) I_1(x) + \text{sgn}(E_{\xi 1s}) I_2(x)] - \frac{\xi}{8\pi l^2} (A_1 - A_2) \tilde{V}_{\text{IL}}(0), \quad (22)$$

$$E_{\xi 1s} = -\mu_0 + sZ - \xi\tilde{\Delta}_0 + \frac{\hbar^2}{2ml^2} [\text{sgn}(E_{\xi 0s}) I_2(x) + \text{sgn}(E_{\xi 1s}) I_3(x)] - \frac{\xi}{8\pi l^2} (A_1 - A_2) \tilde{V}_{\text{IL}}(0). \quad (23)$$

The filling factor

$$\nu = -\frac{1}{2} \sum_{\xi ns} \text{sgn}(E_{\xi ns}) = -\frac{1}{2} (A_1 + A_2) \quad (24)$$

takes values $0, \pm 1, \pm 2, \pm 3 \pm 4$. In general, there are many solutions of the gap equations (22) and (23) at a fixed filling factor ν . The density of the thermodynamical potential of the system for each solution can be calculated by using the BK effective action (8) and the fact that solutions are extrema of this action. We find

$$\begin{aligned} \Omega &= -i \int \frac{d\omega}{8\pi^2 l^2} \sum_{\xi ns} \left\{ \frac{\omega - \mu_0 + sZ - \xi\tilde{\Delta}_0}{\omega - E_{\xi ns} + i\delta \text{sgn}\omega} - 1 \right\} \\ &= -\frac{1}{8\pi l^2} \sum_{\xi=\pm} \sum_{s=\pm} \sum_{n=0,1} [E_{\xi ns} - \mu_0 + sZ - \xi\tilde{\Delta}_0] \text{sgn}(E_{\xi ns}). \end{aligned} \quad (25)$$

IV. SOLUTIONS AND PHASE DIAGRAM IN THE LOWEST LANDAU LEVEL

The chemical potential is one of thermodynamic variables of the thermodynamic potential (25). However, in experiments with bilayer graphene, the top and/or bottom gates control the charge density (filling factor ν) rather than the chemical potential. Therefore, it is convenient to perform a Legendre transform and use the charge density as a thermodynamic variable.

Usually, there is a one-to-one correspondence between the chemical potential of a system and its charge density. However, in the case under consideration, such a correspondence is absent. Indeed, since we consider an ideal system

at zero temperature and zero LLL width, the chemical potential can take arbitrary values within the gap between the filled and unfilled levels. Since the LLL states corresponding to the filling factors $\nu = 0, \pm 1, \pm 2$, and ± 3 are gapped, this is a general situation in the present dynamics.

Actually, this simplifies the analysis of these states: because as soon as the filling factor is fixed, the chemical potential becomes an irrelevant parameter and does not affect the energy density of the system for any solution studied. Explicitly, using the charge density

$$\rho = i \int_{-\infty}^{+\infty} \frac{d\omega}{2\pi} \text{tr} [\tilde{G}(\omega; 0)] = -\frac{1}{4\pi l^2} \sum_{\xi=\pm} \sum_{s=\pm} \sum_{n=0,1} \text{sgn}(E_{\xi ns}) \quad (26)$$

and performing the Legendre transform, we find the following free energy density:

$$\mathcal{E} = \Omega + \mu_0 \rho = -\frac{1}{8\pi l^2} \sum_{\xi=\pm} \sum_{s=\pm} \sum_{n=0,1} \left[E_{\xi ns} + \mu_0 + sZ - \xi \tilde{\Delta}_0 \right] \text{sgn}(E_{\xi ns}). \quad (27)$$

Since $-\mu_0$ additively enters $E_{\xi ns}$ defined in Eqs.(22) and (23), it is clear that μ_0 cancels out in (27) for all solutions with a given filling factor.

Therefore, our strategy in the analysis of the gap equations is the following one: At each fixed filling factor ν and given values of the controlling parameters B and E_{\perp} , we find all possible solutions of Eqs. (22) and (23) with a chemical potential allowed by the filling ν , and then determine the ground state as the solution with the lowest free energy density (27).

The gap equations (22) and (23) form a system of algebraic equations for the eight energies $E_{\xi 0s}$ and $E_{\xi 1s}$ of quasiparticle levels. The solutions having the same filling factor differ in the signs of particular energies but have the same combined values of $A_1 + A_2$ (and consequently ν). Therefore in order to describe the solutions corresponding to different filling factors ν , it is sufficiently to specify only the signs of their energies.

By pre-setting the signs of the energies, one finds that for $\nu = 0, \pm 1, \pm 2, \pm 3$, and ± 4 , there are $\binom{8}{4} = 70$, $\binom{8}{3} = 56$, $\binom{8}{2} = 28$, $\binom{8}{1} = 8$, and $\binom{8}{0} = 1$ solutions, respectively. Therefore there are 256 solutions all together. In what follows, we will consider the solutions only with filling factors from 0 to +4 (the solutions with negative values of ν can be obtained from these ones by choosing opposite values of the signs of the energies). This reduces the number of the solutions to 163. For concreteness, we also choose positive values for a magnetic field, $B > 0$, and nonnegative values for an applied electric field, $E_{\perp} \geq 0$.

As is discussed below, the analysis of Eqs. (22), (23) and (27) with a chemical potential allowed by the filling ν ³⁷ shows that for each filling factor, there are only one or two major solutions that have the lowest energy density and therefore are relevant for the phase diagram. Only for $\nu = 1$ and $\nu = 3$, and in a very narrow region of the values of B and E_{\perp} (where the major phases do not exist), there might exist some additional (marginal) phases.

In this section, the properties of the solutions of gap equations (22)-(23) will be described. The comparison of these solutions with experiment will be considered in Sec. V.

A. The $\nu = 0$ QH state

The solutions of the gap equations at the neutral point were analyzed in Refs. [16,17]. Here we briefly describe those results.

There are two competing solutions: I) the ferromagnetic (or spin polarized (SP)) solution and II) the ferroelectric (or layer polarized (LP)) solution. The signs of the energies $E_{\xi ns}$ in the ferromagnetic solution are negative for the states with a spin opposite to magnetic field and positive for the states with a spin along magnetic field:

$$\begin{aligned} \text{sgn}(E_{1,0,-}) &= -1, \text{sgn}(E_{-1,0,-}) = -1, \text{sgn}(E_{1,1,-}) = -1, \text{sgn}(E_{-1,1,-}) = -1, \\ \text{sgn}(E_{1,0,+}) &= 1, \text{sgn}(E_{-1,0,+}) = 1, \text{sgn}(E_{1,1,+}) = 1, \text{sgn}(E_{-1,1,+}) = 1. \end{aligned} \quad (28)$$

In the LP solution, the signs of the energies are correlated with the signs of the valley index ξ (recall that the valley and layer indices are equivalent in the LLL):

$$\begin{aligned} \text{sgn}(E_{1,0,-}) &= -1, \text{sgn}(E_{1,0,+}) = -1, \text{sgn}(E_{1,1,-}) = -1, \text{sgn}(E_{1,1,+}) = -1, \\ \text{sgn}(E_{-1,0,-}) &= 1, \text{sgn}(E_{-1,0,+}) = 1, \text{sgn}(E_{-1,1,-}) = 1, \text{sgn}(E_{-1,1,+}) = 1. \end{aligned} \quad (29)$$

The analytical expressions for the energies $E_{\xi ns}$ of these two solutions can be easily found from Eqs.(22) and (23). Then, from Eq. (27) with $\mu_0 = 0$,³⁷ one finds their energy densities:

$$\mathcal{E}_{\text{SP}} = -\frac{2}{\pi l^2} \left(Z + \frac{\hbar^2}{8ml^2} (I_1 + 2I_2 + I_3) \right) \quad (30)$$

and

$$\mathcal{E}_{\text{LP}} = -\frac{2}{\pi l^2} \left(\tilde{\Delta}_0 - \frac{e^2 d}{\kappa l^2} + \frac{\hbar^2}{8ml^2} (I_1 + 2I_2 + I_3) \right), \quad (31)$$

where the integrals I_i are defined in Eq. (21) and the dielectric constant κ is a free parameter in this model. Comparing

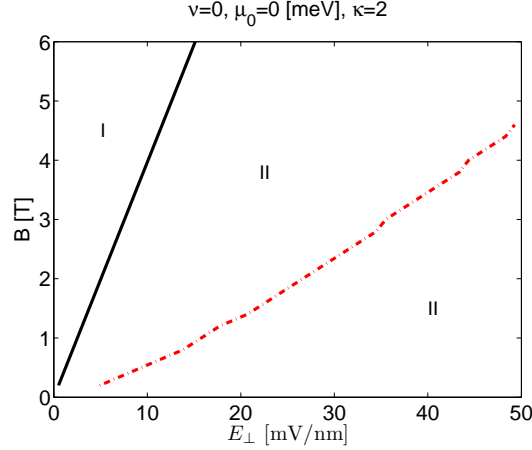


FIG. 1: The phase diagram for the $\nu = 0$ QH state in the (E_{\perp}, B) plane. Here the dielectric constant $\kappa = 2$.

the expressions for \mathcal{E}_{SP} and \mathcal{E}_{LP} , one concludes that there is a critical line separating the SP and LP phases in the $\tilde{\Delta}_0 B$ plane:^{16,17}

$$\tilde{\Delta}_0^{\text{cr}} = Z + \frac{e^2 d}{\kappa l^2}. \quad (32)$$

In order to compare our results with experimental data in Refs. 7–10, it is convenient to express the top-bottom gates voltage imbalance $\tilde{\Delta}_0$ through the electric field, $E_{\perp} = 2\tilde{\Delta}_0/ed$. Then, the critical line in the $E_{\perp} B$ plane takes the form

$$E_{\perp}^{\text{cr}} = \frac{2}{ed} \left(Z + \frac{e^2 d}{\kappa l^2} \right). \quad (33)$$

Using $Z \simeq 0.67 B[\text{T}]\text{K}$ and $l = \sqrt{\hbar c/eB}$, this relation can be rewritten as

$$E_{\perp}^{\text{cr}} [\frac{\text{mV}}{\text{nm}}] \simeq (0.33 + \frac{4.4}{\kappa}) B[\text{T}]. \quad (34)$$

We plot the phase diagram of the $\nu = 0$ state in Fig. 1 (compare with Refs. 16,17). The I (II) area is that where the SP (LP) solution is favorite. The red dashed line and the B axis compose the boundary of the region where the two solutions coexist: the solution I does not exist to the right of the (red) dashed line in the region II. The black bold line is a critical line between the phases I and II. For balanced bilayer ($E_{\perp} = 0$), the SP solution is favorite due to the presence of the Zeeman term. At fixed B for sufficiently large electric field E_{\perp} , the LP solution is realized.

The gap $\Delta_{\nu=0}$ for the Hall state $\nu = 0$ is equal to the difference between the lowest empty (positive energy) level and the highest filled (negative energy) level. For the SP solution, it is

$$\Delta_{\nu=0} = E_{1,1,+} - E_{-1,1,-} = 2 \left[Z - \frac{ed}{2} E_{\perp} + \frac{\hbar^2}{2ml^2} (I_2 + I_3) \right], \quad E_{\perp} < \frac{2}{ed} [Z + \frac{\hbar^2}{2ml^2} (I_2 + I_3)], \quad (35)$$

and

$$\Delta_{\nu=0} = E_{-1,1,-} - E_{1,1,+} = 2 \left[-Z + \frac{ed}{2} E_{\perp} + \frac{\hbar^2}{2ml^2} (I_2 + I_3) - \frac{2e^2 d}{\kappa l^2} \right], \quad E_{\perp} > \frac{2}{ed} \left[Z - \frac{\hbar^2}{2ml^2} (I_2 + I_3) + \frac{e^2 d}{\kappa l^2} \right] \quad (36)$$

for the LP solution.

At a fixed value of the magnetic field, the SP gap decreases with increasing E_{\perp} up to the point $E_{\perp} = 2[Z + \hbar^2/2ml^2(I_2 + I_3)]/ed$, where it vanishes. On the other hand, the LP gap always increases with E_{\perp} . According to the expression in Eq. (33) for the critical line, the SP solution is favored for $E_{\perp} < E_{\perp}^{\text{cr}}$, while at $E_{\perp} > E_{\perp}^{\text{cr}}$ the LP solution is realized. At the critical line, the gaps of the two phases coincide and are given by

$$\Delta_{\nu=0}^{\text{cr}} = \frac{\hbar^2}{ml^2} \left(I_2 + I_3 - \frac{2e^2 dm}{\kappa \hbar^2} \right). \quad (37)$$

Let us describe the phase transition between the SP and LP phases in more detail. In Fig. 2, the gap $\Delta_{\nu=0}$ and the energy spectrum $E_{\xi ns}$ are shown as functions of the electric field E_{\perp} at the fixed value of the magnetic field $B = 2$ [T]. The critical value of E_{\perp} is $E_{\perp}^{\text{cr}} \simeq 5.04$ mV/nm and $\Delta_{\nu=0}^{\text{cr}} \simeq 3.73$ meV in this case.

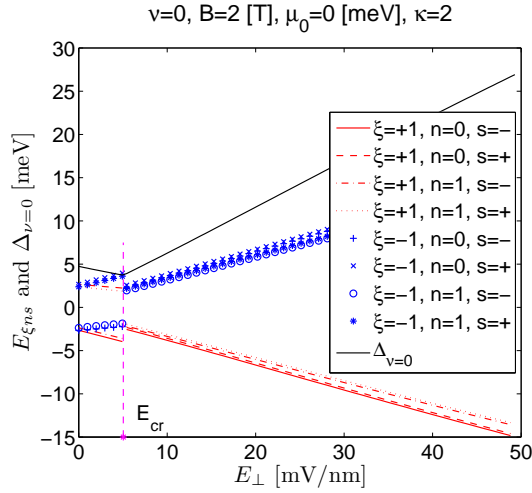


FIG. 2: The energy spectrum and the gap of the $\nu = 0$ QH state as functions of the electric field at the fixed magnetic field $B = 2$ [T]. Here the dielectric constant $\kappa = 2$.

As one can see in Fig. 2, ignoring a small splitting of the LLs due to the electric field, the symmetry of the SP phase at $E_{\perp} < E_{\perp}^{\text{cr}}$ is $G_2 = U^{(K)}(1)_+ \times U^{(K)}(1)_- \times U^{(K')}(1)_+ \times U^{(K')}(1)_- \times Z_{2V}^{(+)} \times Z_{2V}^{(-)}$ considered in Sec. II. Now, at the critical value E_{\perp}^{cr} , a jump in the energy spectrum takes place (see Fig. 2). Since the value of the gap $\Delta_{\nu=0}^{\text{cr}}$ at $E_{\perp} = E_{\perp}^{\text{cr}}$ is nonzero, this leads to a jump transformation of the G_2 symmetry into the $U^{(K)}(2)_S \times U^{(K')}(2)_S$ one at $E_{\perp} > E_{\perp}^{\text{cr}}$ (the LP phase), if the Zeeman term is ignored. The presence of such a jump suggests that this phase transition is a discontinuous (first order) one.³⁸

A noticeable feature of this transition is a kink singularity in the gap with a minimum at $E_{\perp} = E_{\perp}^{\text{cr}}$ clearly seen in Fig. 2. As will be discussed in Sec. V, this fact is important for understanding the behavior of the two-terminal conductance in the experiment in Ref. 7. It is interesting that as shown in Appendix, the last term in the Hamiltonian (2), which is responsible for the bare splitting of the Landau levels with $n = 0$ and $n = 1$, transforms the kink singularity into a (stronger) jump one. Although for magnetic fields $B < 10$ T, which are relevant for the present analysis, this jump is very small, it could become relevant for dynamics with higher magnetic fields.

B. The $\nu = 1$ QH state

There are two main solutions at the $\nu = 1$ filling factor (see Fig. 3). The first solution is:

$$\text{sgn}(E_{1,0,-}) = -1, \text{sgn}(E_{-1,0,-}) = -1, \text{sgn}(E_{1,1,-}) = -1, \text{sgn}(E_{-1,1,-}) = -1,$$

$$\text{sgn}(E_{1,0,+}) = -1, \text{sgn}(E_{-1,0,+}) = 1, \text{sgn}(E_{1,1,+}) = 1, \text{sgn}(E_{-1,1,+}) = 1. \quad (38)$$

This solution is closely connected with the SP one in Eq. (28). It differs from the latter only in that its LL with $\xi = 1, n = 0, s = +$ is filled. It would be appropriate to call this solution a partially spin polarized (PSP) one.

The second solution is:

$$\begin{aligned} \text{sgn}(E_{1,0,-}) &= -1, \text{sgn}(E_{1,0,+}) = -1, \text{sgn}(E_{1,1,-}) = -1, \text{sgn}(E_{1,1,+}) = -1, \\ \text{sgn}(E_{-1,0,-}) &= -1, \text{sgn}(E_{-1,0,+}) = 1, \text{sgn}(E_{-1,1,-}) = 1, \text{sgn}(E_{-1,1,+}) = 1. \end{aligned} \quad (39)$$

It is closely connected with the LP solution in Eq. (29). The difference is in that the LL with $\xi = -1, n = 0, s = -$ is now filled. It would be appropriate to call this solution a partially layer polarized (PLP) one.

The energy densities of the partially filled spin polarized and layer polarized solutions are given by:

$$\mathcal{E}_{\text{PSP}} = -\frac{1}{2\pi l^2} \left[3Z + \frac{\hbar^2}{2ml^2}(I_1 + I_2 + I_3) - \frac{e^2 d}{4\kappa l^2} + \frac{eE_{\perp}d}{2} \right] \quad (40)$$

and

$$\mathcal{E}_{\text{PLP}} = -\frac{1}{2\pi l^2} \left[Z + \frac{\hbar^2}{2ml^2}(I_1 + I_2 + I_3) - \frac{9e^2 d}{4\kappa l^2} + \frac{3eE_{\perp}d}{2} \right], \quad (41)$$

respectively. Comparing these two energy densities, we conclude that the critical line between the PSP and PLP solutions exactly coincides with that between the SP and LP ones (see Eq. (34)). It is quite noticeable that this result is in complete accord with experimental data in Ref. 7 according to which the phase transition between the two $\nu = +1$ states takes place near the same electric field at which the transition between the two $\nu = 0$ states is observed.

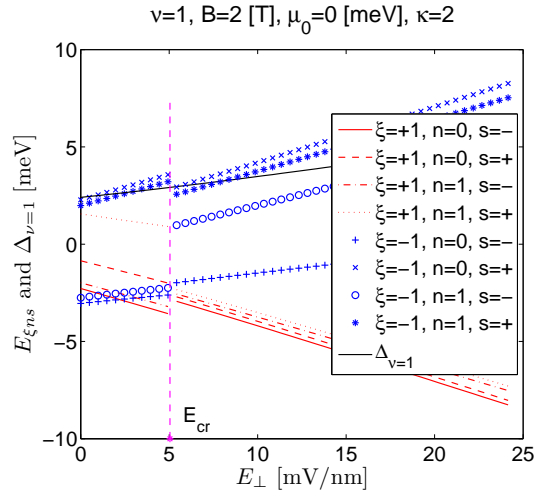


FIG. 3: The energy spectrum and the gap of the $\nu = 1$ QH state as functions of the electric field at the fixed magnetic field $B = 2$ [T]. Here the dielectric constant $\kappa = 2$.

The gap $\Delta_{\nu=1}$ and the energy spectrum $E_{\xi ns}$ for the $\nu = 1$ QH state are shown in Fig. 3. As one can see, a jump in the spectrum at $E_{\perp} = E_{\perp}^{\text{cr}} \simeq 5.04 \text{ mV/nm}$ is similar to that in the $\nu = 0$ QH state. The phase transition at $E_{\perp} = E_{\perp}^{\text{cr}}$ corresponds to the transformation of the $U^{(K)}(1)_{+} \times U^{(K)}(1)_{-} \times U^{(K')}(1)_{+} \times U^{(K')}(1)_{-} \times Z_{2V}^{(-)}$ symmetry in the PSP phase into the $U^{(K)}(2)_{\mathcal{S}} \times U^{(K')}(1)_{+} \times U^{(K')}(1)_{-}$ in the PLP one (as in the $\nu = 0$ case, we ignore small splittings in the spectrum due to the Zeeman term and the electric field).

As to the energy gap, there is an essential difference in its behavior in comparison with the $\nu = 0$ gap. The energy gap for the PSP solution is found to be

$$\Delta_{\nu=1} = E_{1,1,+} - E_{1,0,+} = \frac{\hbar^2}{2ml^2}(I_1 + I_3 - 2I_2) \quad (42)$$

in the region $E_{\xi ns} < E_{\perp}^{\text{cr}}$, where it is the ground state. In the region $E_{\xi ns} > E_{\perp}^{\text{cr}}$, where the PLP solution is the ground state, the energy gap takes the same form:

$$\Delta_{\nu=1} = E_{-1,1,-} - E_{-1,0,-} = \frac{\hbar^2}{2ml^2}(I_1 + I_3 - 2I_2). \quad (43)$$

As a result, the gap in the ground state is a smooth function of E_\perp (without a kink), unlike the $\nu = 0$ case. As will be discussed in Sec. V, this feature and the phase transition at $E_\perp = E_\perp^{\text{cr}}$ are important for understanding the behavior of the conductance at $\nu = 1$.

Note that both gap (42) and gap (43) are expressed as differences of the LL energies with different orbital number n . This takes place also for the $\nu = 3$ QH state (see Sec. IVD below). The polarization of the LLs states with different orbital numbers at odd-integer filling factors was predicted in Ref.11 based on the Hund's rule.

The following remark is in order. In addition to the two solutions described above, there are also two other, marginal, solutions. The first of them is the same as the PSP solution (38) except that instead the state with $\xi = 1$, $n = 0$, $s = +$, it has the state with $\xi = 1$, $n = 1$, $s = +$ being filled. The second marginal solution is the same as the PLP solution (39) except that the state with $\xi = -1$, $n = 1$, $s = -$ is filled instead that with $\xi = -1$, $n = 0$, $s = -$. These marginal solutions have higher energy density than solutions (38) and (39), however, they exist in a slightly larger region. Therefore, the marginal solutions can describe the ground state of the system only in a small region. This issue will be considered in detail elsewhere.

At last, we comment on how the bare splitting of the Landau levels with orbital indices 0 and 1, discussed in Appendix, influences the $\nu = 1$ solution. First of all, the value of the critical electric field in the $\nu = 1$ state remains the same as in the $\nu = 0$ one. Also, as in the $\nu = 0$ case, the bare splitting leads to a jump in the $\nu = 1$ gap at the critical point. Its value coincides with that in the $\nu = 0$ gap. Although the jump is very small for magnetic fields $B < 10\text{T}$, it could be relevant for dynamics with stronger magnetic fields.

C. The $\nu = 2$ QH state

There is only one solution that describes the ground state at the filling factor $\nu = 2$ (see Fig. 4):

$$\begin{aligned} \text{sgn}(E_{1,0,-}) &= -1, \text{sgn}(E_{-1,0,-}) = -1, \text{sgn}(E_{1,1,-}) = -1, \text{sgn}(E_{-1,1,-}) = -1, \\ \text{sgn}(E_{1,0,+}) &= -1, \text{sgn}(E_{1,1,+}) = -1, \text{sgn}(E_{-1,0,+}) = 1, \text{sgn}(E_{-1,1,+}) = 1. \end{aligned} \quad (44)$$

It can be obtained from the PSP solution (38) in the $\nu = 1$ QH state by filling the LLs with $\xi = 1$, $n = 1$, $s = +$ or, alternatively, from the PLP solution (39) by filling the LLs with $\xi = -1$, $n = 1$, $s = -$. In fact, perhaps more clear understanding of this solution can be obtained by considering the SP and LP solutions in the $\nu = 0$ QH state. For the SP solution (28), its LLs are spin polarized and the LLs with $s = -$ are filled. For the LP solution (29), its LLs are layer polarized and the LLs with $\xi = 1$ are filled. Solution (44) can be obtained from the SP one by filling the LLs with $\xi = 1$ or, alternatively, from the LP solution by filling the LL with $s = -$. It would be appropriate to call it a partially spin-layer polarized (PSLP) solution. The energy density of this solution is

$$\mathcal{E}_{\nu=2} = -\frac{1}{\pi l^2} \left[Z + \frac{\hbar^2}{4ml^2}(I_1 + 2I_2 + I_3) - \frac{e^2 d}{2\kappa l^2} + \frac{eE_\perp d}{2} \right]. \quad (45)$$

The gap $\Delta_{\nu=2}$ and the energy spectrum $E_{\xi ns}$ for the $\nu = 2$ QH state are shown in Fig. 4. The gap is

$$\Delta_{E_\perp < E_\perp^{\text{cr}}} = E_{-1,1,+} - E_{1,1,+} = eE_\perp d + \frac{\hbar^2}{ml^2} \left(I_2 + I_3 - \frac{2e^2 dm}{\kappa \hbar^2} \right) \quad (46)$$

at $E_\perp < E_\perp^{\text{cr}} \simeq 5.04\text{mV/nm}$, and

$$\Delta_{E_\perp > E_\perp^{\text{cr}}} = E_{-1,1,+} - E_{-1,1,-} = 2Z + \frac{\hbar^2}{ml^2} (I_2 + I_3) \quad (47)$$

at $E_\perp > E_\perp^{\text{cr}}$. Note, that at $E_\perp = 0$ the gap $\Delta_{\nu=2}$ (46) is smaller than the gap $\Delta_{\nu=0}$ (35) due to the negative Hartree contribution.

As one can see, unlike the $\nu = 0$ and $\nu = 1$ QH states, there is no jump in the $\nu = 2$ energy spectrum. Instead, a LLs crossing takes place when the electric field E_\perp is between 3.45 mV/nm and 6.41 mV/nm. For all values of E_\perp , the symmetry of the $\nu = 2$ QH state is $U^{(K)}(2)_S \times U^{(K')}(1)_+ \times U^{(K')}(1)_-$, if small splittings in the spectrum due to the Zeeman term are ignored.

As in the $\nu = 0$ QH state, there is a kink in the $\Delta_{\nu=2}$ gap at $E_\perp = E_\perp^{\text{cr}} \simeq 5.04\text{mV/nm}$, however, its structure is quite different: While there is a minimum in $\Delta_{\nu=0}$ at $E_\perp = E_\perp^{\text{cr}}$, there is no either minimum or maximum in $\Delta_{\nu=2}$ at this same point (compare Figs. 2 and 4). As will be discussed in Sec. V, this fact is important for understanding the behavior of the conductance at $\nu = 2$.

The influence of the bare splitting term of the $n = 0$ and $n = 1$ LLs on the $\nu = 2$ state is described in Appendix. This term leads to the crossing value E_\perp^{cross} that is different from the critical value E_\perp^{cr} in the $\nu = 0$ and $\nu = 1$ states, although their difference is small for $B < 10\text{T}$. The kink singularity in the $\nu = 2$ gap remains unchanged.

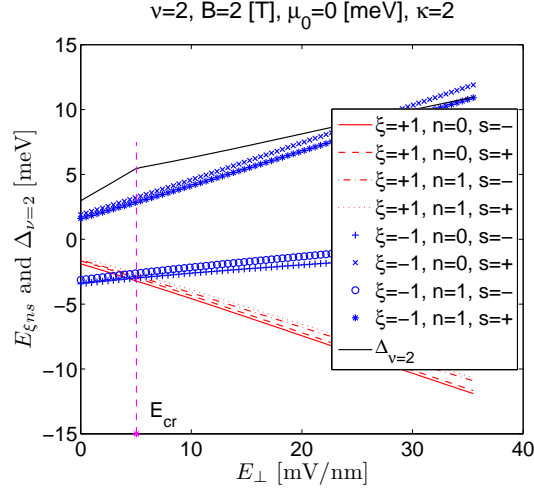


FIG. 4: The energy spectrum and the gap of the $\nu = 2$ QH state as functions of the electric field at the fixed magnetic field $B = 2$ [T]. Here the dielectric constant $\kappa = 2$.

D. The $\nu = 3$ QH state

There is one main solution and two marginal ones in this case. The latter will be considered elsewhere. As to the main solution, it is given by (see Fig. 5)

$$\text{sgn}(E_{1,0,-}) = -1, \text{sgn}(E_{1,0,+}) = -1, \text{sgn}(E_{1,1,-}) = -1, \text{sgn}(E_{1,1,+}) = -1, \quad (48)$$

$$\text{sgn}(E_{-1,0,-}) = -1, \text{sgn}(E_{-1,0,+}) = -1, \text{sgn}(E_{-1,1,-}) = -1, \text{sgn}(E_{-1,1,+}) = 1. \quad (49)$$

It can be obtained from the PSLP solution (44) in the $\nu = 2$ QH state by filling the LLs with orbital $n = 0$ and $\xi = -1$, $s = +$. Its energy density is

$$\mathcal{E}_{\nu=3} = -\frac{1}{2\pi l^2} \left[Z + \frac{eE_{\perp}d}{2} + \frac{\hbar^2}{2ml^2}(I_1 + I_2 + I_3) - \frac{e^2d}{4\kappa l^2} \right]. \quad (50)$$

The gap $\Delta_{\nu=3}$ and the energy spectrum $E_{\xi ns}$ for the $\nu = 3$ QH state are shown in Fig. 5. The gap is

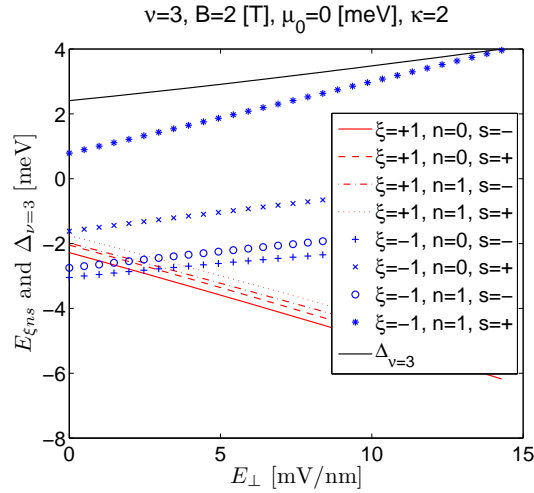


FIG. 5: The energy spectrum and the gap of the $\nu = 3$ QH state as functions of the electric field at the fixed magnetic field $B = 2$ [T]. Here the dielectric constant $\kappa = 2$.

$$\Delta_{\nu=3} = E_{-1,1,+} - E_{-1,0,+} = \frac{\hbar^2}{2ml^2} (I_1 + I_3 - 2I_2) \quad (51)$$

for all values of E_{\perp} .

One can see in Fig. 5 that as in the $\nu = 2$ QH state, there is no jump in the $\nu = 3$ energy spectrum. Instead, a LLs crossing takes place when the electric field E_{\perp} is between 1.48 mV/nm and 3.45 mV/nm. The symmetry of the $\nu = 3$ QH state is the same as that of the $\nu = 2$ one, $U^{(K)}(2)_S \times U^{(K')}(1)_+ \times U^{(K')}(1)_-$ (if small splittings in the spectrum due to the Zeeman term are ignored). The important difference between these two QH states is that the $\Delta_{\nu=3}$ gap in Eq. (51) is expressed as a difference of the LL energies with different orbital number n (similarly to the gaps of the $\nu = 1$ state). Therefore we will call this solution a partially spin-layer-orbital (PSLOP) polarized one.

As in the case of the $\nu = 1$ QH state, there is no kink in the gap $\Delta_{\nu=3}$. This fact is relevant for understanding the behavior of the $\nu = 3$ conductance discussed in Sec. V. As shown in Appendix, the influence of the bare splitting term of the $n = 0$ and $n = 1$ LLs on the $\nu = 3$ state is reduced to adding a small (for $B < 10$ T) term in the gap.

E. The $\nu = 4$ QH state

The ground state is determined by the following solution in this case:

$$\text{sgn}(E_{1,0,-}) = -1, \text{sgn}(E_{1,0,+}) = -1, \text{sgn}(E_{1,1,-}) = -1, \text{sgn}(E_{1,1,+}) = -1,$$

$$\text{sgn}(E_{-1,0,-}) = -1, \text{sgn}(E_{-1,0,+}) = -1, \text{sgn}(E_{-1,1,-}) = -1, \text{sgn}(E_{-1,1,+}) = -1, \quad (52)$$

where the last empty LL in the PSLOP solution (49) (with $\xi = -1, n = 1, s = +$) is now being filled. Thus, the $\nu = 4$ QH state describes the filled LLL. The energy density of this solution equals

$$\mathcal{E}_{\nu=4} = -\frac{\hbar^2}{4\pi ml^4} (I_1 + 2I_2 + I_3). \quad (53)$$

The energy spectrum $E_{\xi ns}$ for the $\nu = 4$ QH state is shown in Fig. 6. At $E_{\perp} = 0$, its symmetry is $G = U^{(K)}(2)_S \times U^{(K')}(2)_S \times Z_{2V}^{(+)} \times Z_{2V}^{(-)}$ (if small splittings in the spectrum due to the Zeeman term are ignored). At nonzero E_{\perp} , the symmetry becomes $U^{(K)}(2)_S \times U^{(K')}(2)_S$. Obviously, this QH state describes the gap between the LLL and the $n = 2$ LL.

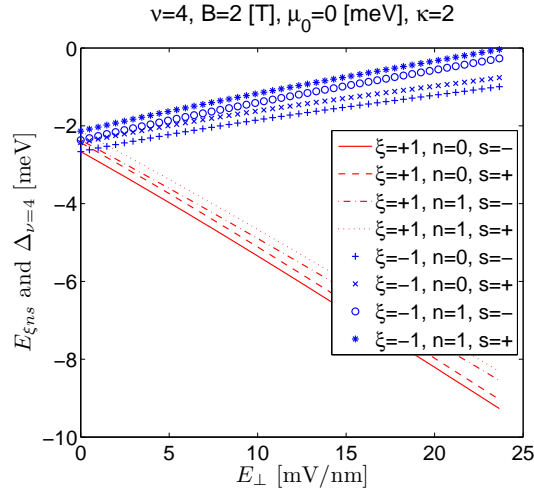


FIG. 6: The energy spectrum of the $\nu = 4$ QH state as a function of the electric field at the fixed magnetic field $B = 2$ [T]. Here the dielectric constant $\kappa = 2$.

V. COMPARISON WITH EXPERIMENT

In this section, we will compare the results of our analysis with the recent experimental data in Refs. 7–10. The comparison is hampered by the presence of disorder in real bilayer samples, which is ignored in the present analysis.

Still, as will be shown below, the results of the analysis reproduce correctly the main characteristics of the experimental data.

Let us start from the critical line between the SP and LP solutions in Eq. (34). One can see that the maximum value of its slope is obtained at the smallest permissible value $\kappa = 1$ for the dielectric constant: it is about $4.7 \text{ mVnm}^{-1} \text{ T}^{-1}$. On the other hand, the value of the slope in experiments^{7,9,10} is about $11 \text{ mVnm}^{-1} \text{ T}^{-1}$. This discrepancy may have its roots in disorder, depending on a type of the latter. For example, an external electric field is more effective in a clean sample (considered in our model) and, therefore, its critical value should be smaller than that in a real sample with charged impurities. On the other hand, neutral impurities might act just in opposite direction by diminishing the role of the Hartree interaction in the gap equations, thus favoring the LP solution. This problem deserves further study.

Let us now turn to the energy gaps as functions of magnetic field at $E_{\perp} = 0$ shown in Fig. 7. Comparing this figure with Fig. 2 in Ref. 8, one can see that the hierarchy of the gaps is the same: $\Delta_{\nu=0} > \Delta_{\nu=2} > \Delta_{\nu=1} = \Delta_{\nu=3}$. Moreover, the theoretical and experimental values of $\Delta_{\nu=0}$ are close. The worst description in the model takes place for the smallest $\Delta_{\nu=1}$ gap: while the experimental $\Delta_{\nu=1}$ is significantly (by factor 10) less than the experimental $\Delta_{\nu=0}$, the gap $\Delta_{\nu=1}$ is twice less than $\Delta_{\nu=0}$ in our model. This fact can be related to the observation in Ref. 8 that the QH states with higher filling factors are subject to additional sources of disorder. Then, it is not unreasonable to assume that the smallest gap, $\Delta_{\nu=1}$, is most sensitive to disorder and therefore suppressed stronger. As to the $\nu = 4$ QH state, it describes a gap between the LLL and the $n = 2$ LL, which is $\Delta_{\nu=4} = \sqrt{2}\hbar\omega_c$, up to small corrections. In

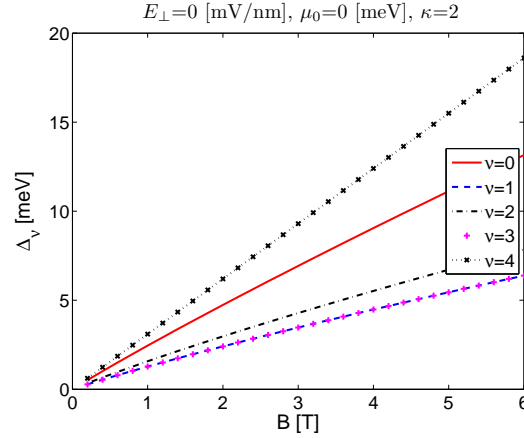


FIG. 7: The energy gaps as functions of magnetic field for different filling factors at zero electric field and $\kappa = 2$.

the rest of this section, we compare the behavior of the energy gaps as functions of electric field in Figs. 2 - 5 with that of the two-terminal conductance in experiment in Ref. 7.

A. Energy gaps and conductance: even ν

One of the main experimental results in Ref. 7 is that the two-terminal conductance is quantized except at particular values of the electric field E_{\perp} . Let us start from the states with even filling factors.

For the $\nu = 0$ state, the experimental data are the following. The conductance in the $\nu = 0$ state is quantized except two values of E_{\perp} , which increase with B .⁷ Let us argue that these two values correspond to $E_{\perp} = \pm E_{\perp}^{\text{cr}}$, where E_{\perp}^{cr} is the critical value at which the phase transition between the SP and LP phases takes place (see Fig. 2; recall that for convenience, we consider only nonnegative values of E_{\perp} in the analysis). As one can see in this figure, the gap $\Delta_{\nu=0}$ has a maximum at $E_{\perp} = 0$ and a minimum at $E_{\perp} = E_{\perp}^{\text{cr}}$. This implies that while the conductivity is suppressed both around zero E_{\perp} and for electric fields larger than E_{\perp}^{cr} , it is enhanced (has a maximum) at $E_{\perp} = E_{\perp}^{\text{cr}}$. This picture agrees with that in Fig. 2C in Ref. 7.

As to E_{\perp}^{cr} , while its experimental value is $E_{\perp}^{\text{cr}} \simeq 29 \text{ mVnm}^{-1}$ at $B = 2.65 \text{ T}$,⁷ it is $E_{\perp}^{\text{cr}} \simeq 6.6 \text{ mVnm}^{-1}$ at $B = 2.65 \text{ T}$ and $\kappa = 2$ in our model (see Sec. IV A). This discrepancy can be traced to the discrepancy between the experimental and theoretical values of the slope of the critical line, which in turn could be caused by disorder in real graphene samples (see the discussion above). As one can read from Eq. (34), the slope of the critical line in our model is $2.5 \text{ mVnm}^{-1} \text{ T}^{-1}$ at $\kappa = 2$ while its experimental value is about $11 \text{ mVnm}^{-1} \text{ T}^{-1}$, i.e., by factor 4.4 larger. Taking this factor into account, we find that it will increase E_{\perp}^{cr} from 6.6 mVnm^{-1} to 29 mVnm^{-1} that agrees with the experimental value.

For the $\nu = 2$ state, the picture is quite different. In this case, the conductance quantization is broken only at $E_{\perp} = 0$.⁷ It agrees with the following facts (see Fig. 4): a) unlike $\nu = 0$, there is only one phase determining the ground state for $\nu = 2$; b) for $\nu = 2$ the gap at $E_{\perp} = 0$ is approximately 30 – 40% less than that for $\nu = 0$ and monotonically increases with E_{\perp} ; c) as already mentioned above, the disorder suppresses the $\nu = 2$ gap stronger than the $\nu = 0$ one. Let us also note that as was observed in Ref. 7, in stronger magnetic fields, $B \gtrsim 7.8\text{T}$, the $\nu = 2$ conductance is quantized even around $E_{\perp} = 0$, i.e., at such large B (and therefore $\Delta_{\nu=2}$), the disorder is not able to break the conductance quantization. As to the $\nu = 4$ state, which describes a large gap between the LLL and the $n = 2$ LL, its conductance is obviously quantized for all E_{\perp} .

B. Energy gaps and conductance: odd ν

The quantization of the conductance of the $\nu = 1$ state is broken at the same finite values of E_{\perp} as those in the $\nu = 0$ one.⁷ It is also broken around $E_{\perp} = 0$. As to the $\nu = 3$ state, the situation is similar to that in the $\nu = 2$ state: the quantization of its conductance is broken only around $E_{\perp} = 0$. It is noticeable that in order to see these effects in the odd ν states, one can use larger values of magnetic field ($B = 3.43\text{T}$ in Ref. 7). This suggests that the odd ν states are more sensitive to disorder than those with even ν .

Let us discuss how these experimental data are reflected in the present analysis. The results for the $\nu = 3$ state, seems to be clear: as in the $\nu = 2$ one, in this case there is one phase describing the ground state and its gap has a minimum only at $E_{\perp} = 0$. The case of the $\nu = 1$ state is more subtle. As for $\nu = 0$, there are two phases describing the ground state (the PSP and PLP ones). Moreover, the critical line dividing these phases exactly coincides with that between the SP and LP ones at $\nu = 0$. This is in accordance with the experimental data. However, unlike the $\nu = 0$ state, there is no minimum in the gap at E_{\perp}^{cr} (see Fig. 3). Instead, the gap is a smooth monotonically increasing function of E_{\perp} and has a minimum only at $E_{\perp} = 0$. This seems to suggest that, in disagreement with experiment, the quantization of the conductance at $\nu = 1$ should be broken only at $E_{\perp} = 0$, *despite the presence of the phase transition at $E_{\perp} = E_{\perp}^{\text{cr}} \simeq 5.04\text{mV/nm}$.*

How can one solve this puzzle? A possible explanation might be as follows. Such a smooth behavior of the $\nu = 1$ gap occurs due to delicate cancellations of different terms in calculating the gap in the PSP and PLP phases. This cancelation could be just an artifact of the approximation used in the present analysis. On the other hand, it may also suggest that although beyond this approximation a dynamics responsible for the conductance quantization breakdown at $E_{\perp} = E_{\perp}^{\text{cr}}$ at $\nu = 1$ does exist, it is weaker than that at $\nu = 0$, *even in perfectly clean samples*. This point deserves further study.

VI. CONCLUSION

In this paper, the analysis of Refs. 16,17 was extended beyond the neutral point with the filling factor $\nu = 0$ to describe the doped QH states with filling factors $\nu = \pm 1, \pm 2, \pm 3$, and $\nu = \pm 4$. It is noticeable that such a relatively simple model as the present one reproduces the main characteristics of experimentally observed broken-symmetry LLL states in a magnetic field. One important ingredient in the model is a very strong screening of the Coulomb interactions described by the polarization function. Such a strong screening radically changes the form of the interaction and is responsible for a linear scaling of dynamical gaps with a magnetic field in bilayer graphene in contrast to monolayer graphene where a \sqrt{B} scaling takes place. The behavior of gaps as functions of magnetic field at zero electric field for different filling factors, Fig.7, is found to be in a good agreement with experimental data.⁸ The amplitudes of the gaps at the $\nu = \pm 1, 3$ and $\nu = \pm 2$ plateaus are significantly smaller than the amplitude of the $\nu = 0$ gap, due to the separate filling of the $n = 0$ and $n = 1$ orbital Landau levels and the negative contribution of the Hartree term, respectively.

At nonzero electric field, we found a critical line in the plane of electric field, E_{\perp} , and magnetic field, B , that separates both the spin and layer polarized phases at $\nu = 0$ and the partially spin and layer polarized phases at $\nu = \pm 1$. On the other hand, there are unique phases for $\nu = \pm 2$ and $\nu = \pm 3$ QH states. The phase transition point moves out to larger electric fields as the magnetic field is increased, which implies that the ferromagnetic phase is stabilized by a magnetic field and is destabilized by an electric field.

By studying the evolution of the gaps with an external electric field, we revealed a strong correlation between this evolution and the behavior of the conductance in the experiment:⁷ the values of the electric field at the minima of the gaps correspond to those ones where the conductance is not quantized. The only exception is the $\nu = \pm 1$ QH state, where the gap has a minimum only at $E_{\perp} = 0$ and not at finite values of the electric field (possible reasons for such a disagreement were considered in Sec. V B).

Finally, we would like to note that as has been recently shown in Ref. 39, nontrivial order parameters can also have important effects on the minimal dc conductivity in bilayer graphene.

Note added: After this work was submitted for publication, a new experimental paper, Ref. 40, has appeared, in which the phase diagram of the $\nu = 0$ QH state in bilayer graphene is studied. In agreement with the theoretical predictions,^{16–19} the critical line observed in that work separates the spin-polarized and layer-polarized states and has the form similar to the theoretical one, except the region with very low values of B , where the LLL approximation is apparently unreliable. In another recent experimental paper,⁴¹ a phase transition to the nematic state was observed in bilayer graphene without magnetic field. The nematic state has been predicted in theoretical works.⁴² It breaks the rotational symmetry and keeps quasiparticles gapless. It would be interesting to study a competition between the gapped state and the nematic state due to the Coulomb interaction and other interactions in bilayer graphene in a magnetic field.

Acknowledgments

V.A.M. acknowledges useful discussions with Giovanni Fanchini. The work of E.V.G. and V.P.G. was supported partially by the Scientific Cooperation Between Eastern Europe and Switzerland (SCOPES) programme under Grant No. IZ73Z0-128026 of the Swiss National Science Foundation (NSF), the European FP7 program, Grant No. SIMTECH 246937, and by the joint Ukrainian-Russian SFFR-RFBR Grant No. F40.2/108. V.P.G. acknowledges a collaborative grant from the Swedish Institute. The work of J.J. and V.A.M. was supported by the Natural Sciences and Engineering Research Council of Canada.

Appendix A: Bare splitting of the Landau levels with $n = 0$ and $n = 1$

In this Appendix, we comment on the splitting of the Landau levels with orbital indices 0 and 1 due to the bias electric field which leads to the sombrero shape of the upper band in the Hamiltonian of four-band model at zero magnetic field.^{1,4,24} Under the reduction to the two-band model, the influence of the high-energy band is taken into account by the last term in the Hamiltonian (2). The bare splitting of the $n = 0$ and $n = 1$ LLs is given by the formula¹ $\delta = edE_{\perp}\hbar\omega_c/\gamma_1 \equiv \tilde{\Delta}_0\bar{\delta}$, where the dimensionless $\bar{\delta}$ is $\bar{\delta} = 2\hbar\omega_c/\gamma_1 \approx 0.011B[\text{T}]$.

This term leads to a modification of the gap equations (22) and (23) for the LLL with $n = 0$ and $n = 1$:

$$\tilde{\Delta}_0 \rightarrow (1 - n\bar{\delta})\tilde{\Delta}_0. \quad (\text{A1})$$

The free energy density (27) of the system will also receive a correction:

$$\mathcal{E} \rightarrow \mathcal{E} = -\frac{1}{8\pi l^2} \sum_{\xi=\pm} \sum_{s=\pm} \sum_{n=0,1} \left[E_{\xi ns} + \mu_0 + sZ - \xi\tilde{\Delta}_0(1 - n\bar{\delta}) \right] \text{sgn}(E_{\xi ns}). \quad (\text{A2})$$

Note that the values of the magnetic field are less than 10T in the experiment with suspended bilayer graphene^{7,8} the results of our analysis are compared with. Therefore in this case the value of $\bar{\delta} = 0.011B[\text{T}]$ is less than 0.1, and all these corrections are small. On the other hand, they could become relevant for stronger magnetic fields.

By combining analytical and numerical methods, the modified gap equations and free energy density were analyzed. Now we list the main results that were obtained in this analysis.

(1) For the $\nu = 0$ state in Sec. IV A, the transformation (A2) corresponds to E_{\perp} in the free energy density of the LP phase effectively transforming as $E_{\perp} \rightarrow (1 - \bar{\delta}/2)E_{\perp}$. Because of that, the critical value E_{\perp}^{cr} separating the SP and LP phases changes:

$$E_{\perp}^{\text{cr}} = \frac{2}{ed(1 - \bar{\delta}/2)} \left(Z + \frac{e^2 d}{\kappa l^2} \right). \quad (\text{A3})$$

The gaps for both the SP and LP phases are modified through the transformation $E_{\perp} \rightarrow (1 - \bar{\delta})E_{\perp}$:

$$\Delta_{\nu=0}^{\text{SP}} = \frac{\hbar^2}{ml^2} (I_2 + I_3) + 2[Z - (1 - \bar{\delta})eE_{\perp}d/2], \quad \Delta_{\nu=0}^{\text{LP}} = \frac{\hbar^2}{ml^2} (I_2 + I_3) - 2[Z + \frac{2e^2 d}{\kappa l^2} - (1 - \bar{\delta})eE_{\perp}d/2]. \quad (\text{A4})$$

As a result, at the critical point, the two gaps will not coincide anymore. Instead, there is a jump in the gap there:

$$\Delta_{\nu=0}^{\text{SP}}(\tilde{\Delta}_0 = \tilde{\Delta}_0^{\text{cr}}) - \Delta_{\nu=0}^{\text{LP}}(\tilde{\Delta}_0 = \tilde{\Delta}_0^{\text{cr}}) = \frac{2\bar{\delta}}{1 - \bar{\delta}/2} \left(Z + \frac{e^2 d}{\kappa l^2} \right). \quad (\text{A5})$$

(2) For the $\nu = 1$ state in Sec. IV B, the transformation (A2) corresponds to E_\perp effectively transforming as $E_\perp \rightarrow (1 - \bar{\delta}/2)E_\perp$ in the free energy density in both the PSP and PLP phases. As a result, the critical value E_\perp^{cr} is modified in the same way as for the $\nu = 0$ state and still coincides with the critical value in the latter. The gaps for the PSP and PLP solutions are modified as:

$$\Delta_{\nu=1}^{\text{PSP}} = \frac{\hbar^2}{2ml^2}(I_1 + I_3 - 2I_2) + \bar{\delta}eE_\perp d/2, \quad \Delta_{\nu=1}^{\text{PLP}} = \frac{\hbar^2}{2ml^2}(I_1 + I_3 - 2I_2) - \bar{\delta}eE_\perp d/2. \quad (\text{A6})$$

Therefore there is also a jump in the gap at the critical point:

$$\Delta_{\nu=1}^{\text{PSP}}(\tilde{\Delta}_0 = \tilde{\Delta}_0^{\text{cr}}) - \Delta_{\nu=1}^{\text{PLP}}(\tilde{\Delta}_0 = \tilde{\Delta}_0^{\text{cr}}) = \frac{2\bar{\delta}}{1 - \bar{\delta}/2} \left(Z + \frac{e^2 d}{\kappa l^2} \right). \quad (\text{A7})$$

It is noticeable that this jump coincides with that in the $\nu = 0$ state (see Eq. (A5)).

(3) For the $\nu = 2$ state, E_\perp in the free energy density also effectively transforms as $E_\perp \rightarrow (1 - \bar{\delta}/2)E_\perp$. There is a crossing of the energy levels $E_{1,1,+}$ and $E_{-1,1,-}$ in this state. As was shown in Sec. IV C, the value of E_\perp^{cross} coincides with that of E_\perp^{cr} in the $\nu = 0$ and $\nu = 1$ states, if the $\bar{\delta}$ correction is ignored. However, when this correction is included, these two values become different. Instead, at the crossing point,

$$E_\perp^{\text{cross}} = \frac{2}{ed(1 - \bar{\delta})} \left(Z + \frac{e^2 d}{\kappa l^2} \right). \quad (\text{A8})$$

The form of the gap for $E_\perp \leq E_\perp^{\text{cross}}$ changes as

$$\Delta_{E_\perp < E_\perp^{\text{cross}}} = (1 - \bar{\delta})eE_\perp d + \frac{\hbar^2}{ml^2} \left(I_2 + I_3 - \frac{2e^2 dm}{\kappa \hbar^2} \right). \quad (\text{A9})$$

The form of the gap for $E_\perp > E_\perp^{\text{cross}}$ remains unchanged. As a result, the kink singularity in the gap at the crossing point also does not change.

(4) For the $\nu = 3$ state in Sec. IV D, the E_\perp in the free energy density effectively transforms again as $E_\perp \rightarrow (1 - \bar{\delta}/2)E_\perp$. The gap in this phase changes to

$$\Delta_{\nu=3} = \frac{\hbar^2}{2ml^2} (I_1 + I_3 - 2I_2) - \bar{\delta}eE_\perp d/2. \quad (\text{A10})$$

-
- ¹ E. McCann and V. I. Fal'ko, Phys. Rev. Lett. **96**, 086805 (2006); E. McCann, D. S. L. Abergel, and V. I. Fal'ko, Solid State Commun. **143**, 110 (2007).
² K. S. Novoselov, E. McCann, S. V. Morozov, V. I. Fal'ko, M. I. Katsnelson, U. Zeitler, D. Jiang, F. Schedin and A. K. Geim, Nature Phys. **2**, 177 (2006).
³ E. A. Henriksen, Z. Jiang, L.-C. Tung, M. E. Schwartz, M. Takita, Y.-J. Wang, P. Kim, and H. L. Stormer, Phys. Rev. Lett. **100**, 087403 (2008).
⁴ A. H. Castro Neto, F. Guinea, N. M. R. Peres, K. S. Novoselov, and A. K. Geim, Rev. Mod. Phys. **81**, 109 (2009).
⁵ B. E. Feldman, J. Martin, and A. Yacoby, Nature Phys. **5**, 889 (2009).
⁶ Y. Zhao, P. Cadden-Zimansky, Z. Jiang, and P. Kim, Phys. Rev. Lett. **104**, 066801 (2010).
⁷ R. T. Weitz, M. T. Allen, B. E. Feldman, J. Martin, and A. Yacoby, Science **330**, 812 (2010).
⁸ J. Martin, B. E. Feldman, R. T. Weitz, M. T. Allen, and A. Yacoby, Phys. Rev. Lett. **105**, 256806 (2010).
⁹ S. Kim, K. Lee, and E. Tutuc, Phys. Rev. Lett. **107**, 016803 (2011).
¹⁰ F. Freitag, J. Trbovic, M. Weiss, and C. Schonenberger, arXiv:1104.3816 [cond-mat.mes-hall].
¹¹ Y. Barlas, R. Cote, K. Nomura, and A. H. MacDonald, Phys. Rev. Lett. **101**, 097601 (2008).
¹² D. S. L. Abergel and Tapash Chakraborty, Phys. Rev. Lett. **102**, 056807 (2009).
¹³ K. Shizuya, Phys. Rev. B **79**, 165402 (2009).
¹⁴ M. Nakamura, E. V. Castro, and B. Dora, Phys. Rev. Lett. **103**, 266804 (2009).
¹⁵ R. Nandkishore and L. Levitov, arXiv:0907.5395 [cond-mat.mes-hall].
¹⁶ E. V. Gorbar, V.P. Gusynin, and V. A. Miransky, JETP Lett. **91**, 314 (2010).
¹⁷ E. V. Gorbar, V.P. Gusynin, and V. A. Miransky, Phys. Rev. B **81**, 155451 (2010).
¹⁸ R. Nandkishore and L. Levitov, arXiv:1002.1966 [cond-mat.mes-hall].
¹⁹ C. Tóke and V. I. Fal'ko, Phys. Rev. B **83**, 115455 (2011).
²⁰ M. Kharitonov, arXiv:1105.5386 [cond-mat.str-el].

- ²¹ Y. Zhang, Z. Jiang, J. P. Small, M. S. Purewal, Y.-W. Tan, M. Fazlollahi, J. D. Chudow, J. A. Jaszczak, H. L. Störmer, and P. Kim, *Phys. Rev. Lett.* **96**, 136806 (2006).
- ²² Z. Jiang, Y. Zhang, H.L. Störmer, and P. Kim, *Phys. Rev. Lett.* **99**, 106802 (2007).
- ²³ The effects of the long-range Coulomb interaction on the shift of the energy levels and optical transitions in biased bilayer graphene in a magnetic field have been previously studied in Ref.12. In that paper, in order to find the energy levels shift, the diagonalization of a many-body Hamiltonian with the Coulomb interaction was performed by using the noninteracting many body basis in the Hilbert space constructed from the single-particle states.
- ²⁴ D. S. L. Abergel, V. Apalkov, J. Berashevich, K. Ziegler, and Tapash Chakraborty, *Advances in Physics* **59**, 261 (2010).
- ²⁵ K. Nomura and A. H. MacDonald, *Phys. Rev. Lett.* **96**, 256602 (2006); K. Yang, S. Das Sarma, and A. H. MacDonald, *Phys. Rev. B* **74**, 075423 (2006); M. O. Goerbig, R. Moessner, and B. Douçot, *Phys. Rev. B* **74**, 161407(R) (2006); J. Alicea and M. P. A. Fisher, *Phys. Rev. B* **74**, 075422 (2006); L. Sheng, D. N. Sheng, F. D. M. Haldane, and L. Balents, *Phys. Rev. Lett.* **99**, 196802 (2007).
- ²⁶ V. P. Gusynin, V. A. Miransky, S. G. Sharapov, and I. A. Shovkovy, *Phys. Rev. B* **74**, 195429 (2006); I. F. Herbut, *Phys. Rev. Lett.* **97**, 146401 (2006); *Phys. Rev. B* **75**, 165411 (2007); J.-N. Fuchs and P. Lederer, *Phys. Rev. Lett.* **98**, 016803 (2007); M. Ezawa, *J. Phys. Soc. Jpn.* **76** (2007) 094701.
- ²⁷ F. D. M. Haldane, *Phys. Rev. Lett.* **61**, 2015 (1988).
- ²⁸ E. V. Gorbar, V.P. Gusynin, and V. A. Miransky, *Low Temp. Phys.* **34**, 790 (2008); E. V. Gorbar, V.P. Gusynin, V. A. Miransky, and I. A. Shovkovy, *Phys. Rev. B* **78**, 085437 (2008).
- ²⁹ V. P. Gusynin, V. A. Miransky, and I. A. Shovkovy, *Phys. Rev. Lett.* **73**, 3499 (1994); *Phys. Rev. D* **52**, 4718 (1995).
- ³⁰ D. V. Khveshchenko, *Phys. Rev. Lett.* **87**, 206401 (2001).
- ³¹ E. V. Gorbar, V. P. Gusynin, V. A. Miransky, and I. A. Shovkovy, *Phys. Rev. B* **66**, 045108 (2002).
- ³² N. . Mermin and H. Wagner, *Phys. Rev. Lett.* **17**, 1133 (1966).
- ³³ D. A. Abanin, P. A. Lee, and L. S. Levitov, *Phys. Rev. Lett.* **96**, 176803 (2006).
- ³⁴ G. Baym and L. P. Kadanoff, *Phys. Rev.* **124**, 287 (1961); J. M. Cornwall, R. Jackiw and E. Tomboulis, *Phys. Rev. D* **10**, 2428 (1974).
- ³⁵ This feature is directly connected with that the valley and layer indices are equivalent in the LLL.
- ³⁶ For arguments justifying the static approximation see Ref. 17.
- ³⁷ Note that because the gap between the filled and unfilled levels in the states with $\nu = 0, \pm 1, \pm 2, \pm 3$, and ± 4 contains zero value of the energy for all relevant values of the magnetic and electric fields (see Figs. 2 - 6), one can choose the value $\mu_0 = 0$ in Eqs. (22) and (23).
- ³⁸ In a first order phase transition, two phases coexist and are perturbatively stable, i.e., they are at least metastable. The latter is still an open issue for the $\nu = 0$ phase transition in bilayer graphene.
- ³⁹ G. Dávid, P. Rakya, L. Oroszlány, and J. Cserti, *Phys. Rev. B* **85**, 041402(R) (2012).
- ⁴⁰ J. Velasco Jr., L. Jing, W. Bao, Y. Lee, P. Kratz, V. Aji, M. Bockrath, C.N. Lau and C. Varma, R. Stillwell, D. Smirnov, Fan Zhang, J. Jung and A.H. MacDonald, arXiv:1108.1609v1 [cond-mat.mes-hall].
- ⁴¹ A. S. Mayorov, D. C. Elias, M. Mucha-Kruczynski, R. V. Gorbachev, T. Tudorovskiy, A. Zhukov, S. V. Morozov, M. I. Katsnelson, V. I. Falko, A. K. Geim, and K. S. Novoselov, *Science* **133**, 860 (2011).
- ⁴² O. Vafek and K. Yang, *Phys. Rev. B* **81**, 041401 (2010); Y. Lemonik, I. L. Aleiner, C. Toke, and V. I. Falko, *Phys. Rev. B* **82**, 201408 (2010).